High resolution wind-tunnel investigation about the effect of street trees on pollutant concentration and street canyon ventilation

Wind-tunnel investigation about the effect of street trees on canyon ventilation

Sofia Fellini[a,*], Massimo Marro[a], Annika Vittoria Del Ponte[b], Marilina Barulli[b], Lionel Soulhac[a], Luca Ridolfi[b], Pietro Salizzoni[a]

[a] *Univ Lyon, INSA Lyon, CNRS, Ecole Centrale de Lyon, Univ Claude Bernard Lyon 1, LMFA, UMR5509, 69621, Villeurbanne France*

[b] *Department of Environmental, Land, and Infrastructure Engineering, Politecnico di Torino, Corso Duca degli Abruzzi 24, 10129 Turin, Italy*

Abstract

Greening cities is a key solution to improve the urban microclimate and mitigate the impact of climate change. However, the effect of tree planting on pollutant dispersion in streets is still a debated topic. To shed light on this issue, we present a wind-tunnel experiment aimed at investigating the effect of trees on street canyon ventilation. An idealized urban district was simulated by an array of blocks, and two rows of model trees were arranged at the sides of a street canyon oriented perpendicularly with respect to the wind direction. Reduced scale trees were chosen to mimic a realistic shape and aerodynamic behaviour. Three different spacings between the trees were considered. A passive scalar was injected from a line source placed at ground level and concentration measurements were performed in the whole canyon. Results show that the presence of trees alters the concentration field in the street with a progressive shift from a nearly two-dimensional to a three-dimensional field depending on tree density. The main finding is that, despite the significant spatial variability of the mean concentration induced by the trees, their presence does not affect the overall ventilation efficiency as the bulk exchange velocity between the street canyon and the overlying atmosphere remains almost constant in the different configurations.

*Corresponding author
Email address: `sofia.fellini@ec-lyon.fr` (Sofia Fellini)

Introduction

Urban vegetation plays a key role for the livability of cities (Bozovic et al., 2017). Beyond its aesthetic role, the presence of vegetation brings numerous environmental benefits in urban areas. Evapotranspiration and shading have cooling effects that mitigate the urban heat island (Oliveira et al., 2011; Georgakis and Santamouris, 2017). The large surface area per unit volume of vegetative structures facilitates particle deposition which acts as a sink for pollutant particles (Litschke and Kuttler, 2008). Moreover, vegetation has a fundamental role in the hydrological cycle: water infiltration in vegetated soils retains stormwater from entering the drainage system, thus reducing the risk of flash floods (Livesley et al., 2016; Busca and Revelli, 2022).

While the social and environmental benefits of vegetation in cities are well recognized, the role of vegetation on pollutant dispersion is still controversial (Janhäll, 2015) and depends on the non-trivial interaction between the flow field, the vegetative elements, and the surrounding built environment (Abhijith et al., 2017). This is particularly true in street canyons, where the turbulent flow field is strongly influenced by the geometry of the canyon, its orientation with respect to the external wind (Soulhac et al., 2008), the presence of obstacles (Buccolieri et al., 2022), and the properties of the building walls, e.g., wall roughness and temperature (Allegrini et al., 2013; Murena and Mele, 2016; Marucci and Carpentieri, 2019; Fellini et al., 2020). The presence of vegetated façades on the building walls, for example, alters the near-wall velocity and may result in a reduction of the turbulent air exchange (Li et al., 2022). Low-level hedges, instead, generally improve the air quality at street level and thus help reducing the dose of pollutants inhaled by pedestrians (Gromke et al., 2016).

The interaction between turbulent flow and vegetation is even more complex in tree-lined avenues, where trees occupy a significant volume of the canyon and their effect on pollutant dispersion depends on the properties and shape of the crowns, the height of the trunks, and the planting pattern (Vos et al., 2013; Huang et al., 2019). A pioneering series of wind-tunnel experiments was performed by Gromke and Ruck (2007, 2009, 2012) to investigate this scenario. In their first studies, trees were modelled as a row of small-scale trees with spherical, permeable crowns on thin stems, placed in the middle of a street canyon of unit height to width ratio H/W (Gromke and Ruck, 2007). The wind was perpendicular to the canyon axis. The flow field within the canyon and the concentration at the canyon walls were explored by varying different properties of the trees (crown diameter, tree height, tree spacing). A relevant increase of concentration at the upwind wall and a slight decrease of concentration at the downwind wall were observed. These variations were more marked when the canyon was occupied by the greatest volume of vegetation (large diameter of crowns and small distance between the trees). To better investigate the effect of tree crown porosity, in a later study, trees were replaced with a metallic cage filled with different amounts of synthetic wadding material (Gromke and Ruck, 2009). They found that concentrations are sensitive to crown porosity only for high porosity values ($> 97\%$). Adopting the same experimental conditions, Buccolieri et al. (2009, 2011) simulated a large street canyon ($H/W = 0.5$) with two rows of trees. They also analysed the case of an approaching wind inclined by $45°$ with respect to the street axis. The aspect ratio of the canyon and the wind direction turned out to be more influential with respect to vegetation density and crown porosity. However, they evidenced that neglecting the presence of vegetation in the streets would lead to significant errors in the predictions of concentration levels.

The modification of the airflow and concentration field within streets due to tree planting has been widely studied also by means of numerical simulations. Reynolds-averaged Navier-Stokes (RANS) models proved to be able to qualitatively reproduce the experimental results (e.g. Gromke et al., 2008; Buccolieri et al., 2009, 2011; Gromke and Blocken, 2015; Vranckx et al., 2015) but Large Eddy Simulations provide a better agreement as they solve the intermittent and unsteady fluctuations of the turbulent flow which plays a major role in ventilation dynamics (e.g., Salim et al., 2011; Moonen et al., 2013). However, the advantages of LES involve higher computational costs that can increase by an order of magnitude compared to RANS (Salim et al., 2011). Merlier et al. (2018) showed that, thanks to its computational efficiency, LES with the lattice Boltzmann method (LBM) is a promising technique to predict dispersion in street canyons with tree plantings.

Despite remarkable advances in numerical models, simulating complex and porous geometries such as trees and their effect on pollutant dispersion still represents a challenge. Wind-tunnel experiments are thus highly recommended to improve and validate existing models. To our knowledge, there is currently no experimental dataset that provides a complete characterization of the concentration field in a three-dimensional street canyon with different configurations of tree planting. For these reasons, we present in this work the results from a wind-tunnel experiment aimed at evaluating how tree planting influences the concentration field within a street canyon. To this aim, we reproduce a street canyon oriented perpendicular with respect to the wind direction, with two lateral rows of trees and a linear source of gas to mimic vehicular emissions. To provide a detailed description of the phenomenon, the concentration field is measured on a high-refined measurement grid with around 1000 sampling points for each configuration of tree density. The reference configuration is that of a canyon closed laterally, i.e. it does not communicate with side streets. Although this is an uncommon configuration, it allows us to accurately estimate the exchange of pollutants between the canyon and the atmosphere above. Experiments have however also been performed in a laterally open canyon, showing that the spatial pattern of concentration is not significantly affected by the presence of lateral openings.

In Section 1, the experimental setup and the adopted measurement techniques are presented. In Section 2, we discuss the similarity criteria for the aerodynamic modelling of trees and for the boundary layer in the wind tunnel. The characterization of the concentration field in the street canyon is reported in Section 3, together with the estimate of the ventilation efficiency. Moreover, the effect of lateral conditions due to different extremities (street intersections, open or closed canyon) is discussed in Section 4. Finally, the conclusions and perspectives of the work are presented in Section 5.

1. Experimental setup and measurement techniques

1.1. Wind-tunnel setup

The experiments were performed in the atmospheric wind tunnel at the laboratory Laboratoire de Mécanique des Fluides et d'Acoustique (LMFA) at the École Centrale de Lyon. The aerodynamic circuit is composed by an axial fan which induces wind velocities between 0.5 and 6 m/s, flow diverging and converging systems, and an upwind grid for the generation of homogeneous turbulence. A heat exchanger system regulates the air temperature with a precision of 0.5 K. The test section of the wind tunnel is 12 m long, 3.5 m wide, and 2 m high.

To simulate an idealized urban district (Fig. 1), the floor of the entire test section was overlaid with an array of square blocks (panel a in Fig. 2). The blocks were 50 cm wide and 10 cm high and made of wood and polystyrene. The spacing between the obstacles was 10 cm in the spanwise direction and 20 cm in the lengthwise direction. In this way, we obtained a street network composed of square canyons (height to width ratio H/W =1) aligned with the wind direction intersecting larger perpendicular streets ($H/W = 0.5$). The two different proportions were selected to avoid channeling effects along the wind direction and to recreate tree-lined boulevards in the direction perpendicular to the wind. The blockage ratio of the model to the cross-section of the wind tunnel was 5%.

A neutrally stratified boundary layer approximately 1.1 m depth was generated by combining the effect of a row of 0.95 m high Irwin spires (Irwin, 1981), placed at the beginning of the test section, and the building-like obstacles on the floor. Moreover, the obstacles were covered by 5 mm high bolts to generate further roughness and accelerate the full development of the boundary layer. The free stream velocity at the top of the boundary layer (U_∞) was kept constant around 5 m/s. More details about the boundary layer above the obstacles is given in Section 2.2.

The reference street canyon (see photo reported in Fig. 2.c) was placed perpendicular to the wind direction, at a distance of approximately 9 meters from the beginning of the test section. Its length (L), width (W), and height (H) measured 1.0 m, 0.2 m, and 0.1 m, respectively (Fig. 2.b and d). In a 1:200 scale, the street canyon matches fairly well a typical tree-lined boulevard, 40 m wide and flanked by 20 m high buildings, as in typical European city centres (e.g., Barcelona, Turin, Lyon). Note that, in the experiment, the length of the canyon does not cover the whole width of the test section. This choice is made in order to define a control volume in which to apply the mass balance for an accurate estimate of the ventilation efficiency (see Section 3.2). We are aware that other boundary conditions are possible, for instance street intersections or an indefinitely long canyon. The effects of different lateral extremities will be discussed in Section 4.

To simulate urban vegetation in the street canyon, model trees were aligned along two lateral rows 14 cm apart. Three different configurations for the tree density were analysed: in configuration *Zero* (panel d), the street canyon was empty. In configuration *Half* (panel e), seven equally spaced trees were arranged along each lateral row. In configuration *Full* (panel f), the lateral rows were composed of fourteen trees with no space between them. The aerodynamic characterization of model trees is reported in Section 2.1.

To simulate vehicular emissions, a tracer was emitted by a linear source at the centre of the reference street canyon. The source consisted of a stainless steel tube pierced with needles emitting ethane in a gas homogenization chamber, located in a slot cut in the tunnel floor. From this chamber the gas was released homogeneously at street level from a 65 cm long and 1 cm wide metallic grid. This design aims at minimizing the vertical momentum and maximize the lateral homogeneity of the emission (Meroney et al., 1996; Marro et al., 2020). Ethane was chosen as a tracer, since it has approximately the same density of air (the density ratio between ethane and air being about 1.03). The source released a mixture of air and ethane with a total flow rate of 4 l/min and thus a negligible

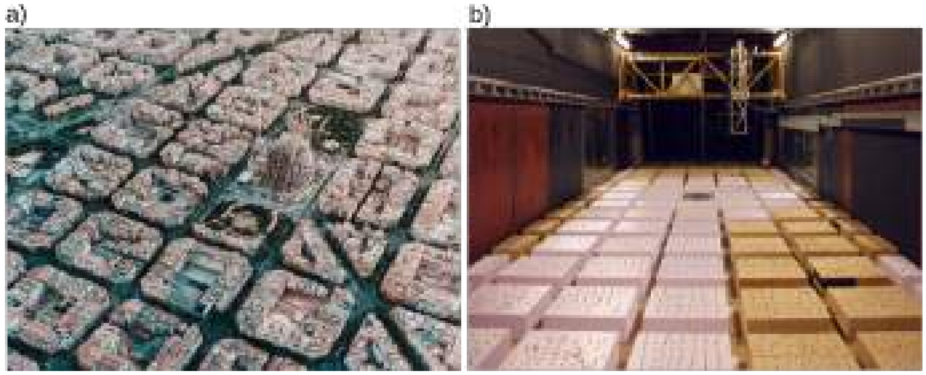

Figure 1: (a) Aerial view of the city of Barcelona (Spain). Source: *Barcelona From Above* by Ian Harper. (b) The modelled urban canopy in the wind tunnel.

injection velocity at street level of approximately 0.01 m/s. The percentage of ethane was around 5% in volume, corresponding to a flow rate of around 0.2 l/min. The supply of the two gases was monitored by two digital mass-flow controllers (Alicat Scientific MC-Series) working in a range between 0.5 and 20 Nl/min.

1.2. Measurement techniques

The concentration field within the reference street canyon was measured using a Flame Ionisation Detector (FID) system (Fackrell, 1980), which is commonly used for measurements in urban-like geometries (Pavageau and Schatzmann, 1999; Carpentieri et al., 2012; Fellini et al., 2020). To avoid the disruption of the local flow, a straight 30 cm long sampling capillary tube was mounted on the FID head, which was positioned above the test section so as not to affect the flow field. The sampling frequency of the FID signal was fixed at 1000 Hz (Nironi et al., 2015). The instrument works in the range 0-10 Volt and it can detect concentration values between 0 and 5000 ppm with an accuracy of about 1-2 ppm.

The measurements were performed in statistically steady conditions: a constant flow rate of ethane was injected from the ground level source and the concentration within the cavity was measured at around 1000 sampling points

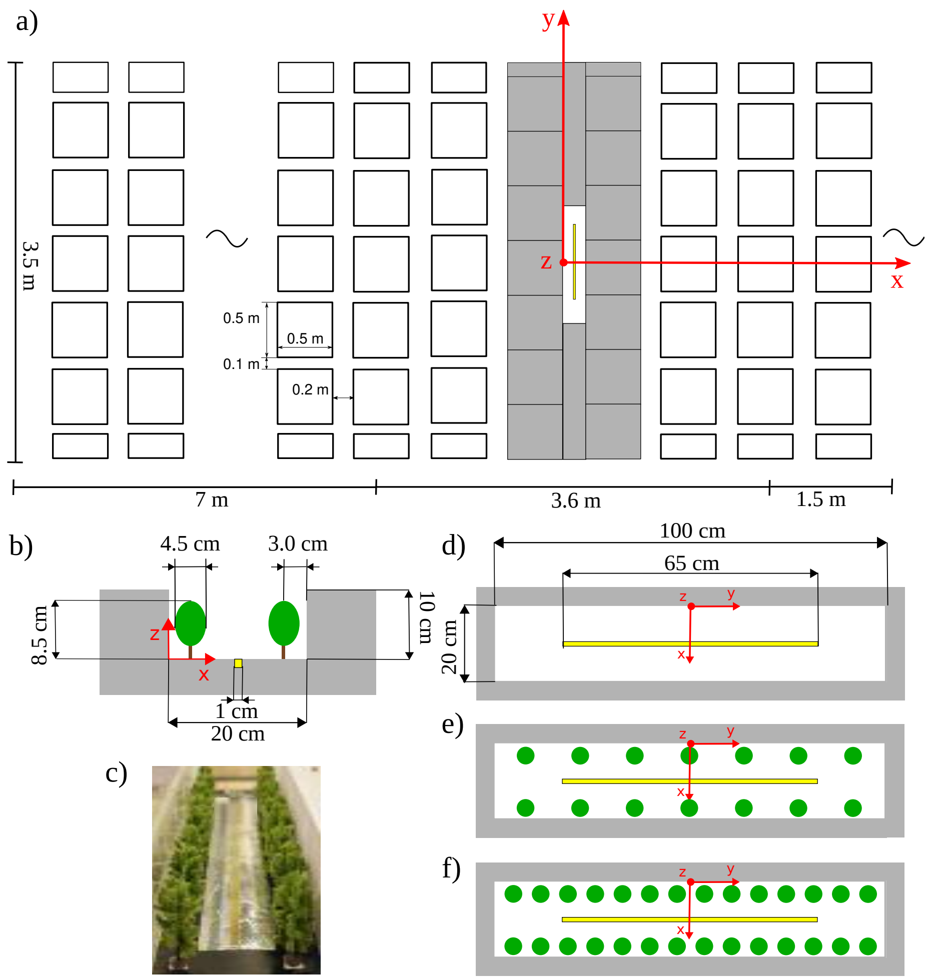

Figure 2: (a) Sketch of the urban canopy in the test section of the tunnel. The blocks delimiting the reference street canyon are coloured grey. Sketch (b) and photo (c) of the front view of the street. Top view of the street canyon model for the different configurations of tree density: (d) *Zero*, (e) *Half*, (f) *Full*. The yellow line represents the pollutant source

for each configuration of tree density. The measurement grid was defined to characterize the entire three-dimensional volume in detail (see Fig. 1 in the Supplementary Material). For each point, we fixed a sampling time of 2 minutes which provides a reliable estimate of the mean concentration. Moreover, before and after each acquisition, the background concentration was recorded by stopping the emission for 15 seconds (and leaving time for the transients to settle). The background concentration, which was assumed to evolve linearly with time from its initial to its final value, was then subtracted from the signals (Marro et al., 2020; Vidali et al., 2022).

The velocity field above the obstacles was characterized (Section 2.2) by means of a Hot-Wire Anemometer (HWA) at constant temperature, using an X-wire probe with acceptance angle of 45°. In this way, two velocity components of the velocity field were measured simultaneously. The platinum probe wire was 1 mm long and with a diameter of 5 μm. The small size of the hot-wire element enables good spatial resolution of the velocity field while the low thermal inertia of the material ensures fast response, allowing the detection of high-frequency fluctuations of the turbulent flow (Comte-Bellot, 1976). An acquisition time of 1 minute at a frequency of 4000 Hz was adopted for each sampling point.

For the aerodynamic characterization of the model trees (presented in Section 2.1), their drag coefficient was measured in a small closed-circuit wind tunnel with a 30 cm x 30 cm test section and able to generate velocities up to 25 m/s. The tunnel was equipped with an external load cell with a precision of 0.01 N. Different layouts of trees were attached to a removable plate connected with the load cell. The drag coefficient was estimated for a varying wind velocity inside the tunnel. Moreover, the aerodynamic porosity of the model trees was evaluated by performing velocity measurements upwind and downwind a single tree on a regular grid by means of a Pitot tube.

2. Similarity criteria

2.1. Aerodynamic characterization of model trees

To investigate the effect of trees in urban areas by means of wind-tunnel experiments, buildings and vegetative structures need to be modelled in small scale. Similarity criteria are then necessary to transfer small-scale findings in the wind tunnel to full-scale applications. For impermeable and rigid structures, like buildings, dynamical similarity between the experiment and the real application exists if the model and the full-scale object are geometrically similar and the value of the Reynolds number is the same (Tritton, 2012). In case of fully turbulent flows around bluff bodies and/or with complex geometries, this condition is weakened and flow similarity is assumed as far as the Reynolds number is sufficiently large. On the other hand, less knowledge is available about the appropriate similarity criteria for vegetative structures. From a fluid dynamical point of view, vegetation is a complex porous medium made of branches and leaves giving rise to the development of boundary layers, wakes, and recirculation zones (Gromke and Ruck, 2008). Moreover, due to their flexibility, trees can sway with the wind and induce fluid-structure interactions.

In previous wind-tunnel experiments, trees, windbreaks, and canopies have been modelled by using different materials, e.g., brushes, cotton balls, metal screens, and plastic stripes. Aerodynamic validation of the adopted structures was done by analysing different fundamental features of the interaction between the trees and the flow field, as the drag coefficient, the characteristics of the wakes behind the trees (Meroney, 1968), the ratio between tree height and roughness length (Meroney, 1980), the leaf area density (Chen et al., 1995), or the sway frequency (Stacey et al., 1994). More systematically, Gromke and Ruck (2008) analysed the aerodynamic characteristics of 12 small-scale modelled trees made of different materials and porosity. Measurements of the drag coefficient and of the flow field around the crowns evidenced the drag coefficient as a key scale parameter for the modelling of trees. Manickathan et al. (2018) compared the aerodynamic behaviour of model and natural trees in a wind tunnel. They found that, together with the drag coefficient, the aerodynamic porosity of the tree crown is another key parameter to compare natural and model trees.

In accordance with these studies, we mimicked natural trees with plastic trees for railway modelling and we characterized their aerodynamic behaviour by estimating their aerodynamic porosity and their drag coefficient. We also investigated their optical porosity. The trees were 8.5 cm high (h_T) and 4.5 cm wide (w_T), with crowns in plastic porous material on plastic trunks. Under the conditions of the experiment, tree models behaved like rigid bodies and thus deformations and fluid-structure interactions could be neglected.

Aerodynamic porosity (α_p) is defined (Guan et al., 2003) as the ratio of the time average wind speed behind the obstacle (U_b) and the average speed of the approaching wind (U_{ref}):

$$\alpha_p = \frac{\int_{A_c} U_b(x,y)dA_c}{\int_{A_c} U_{ref}(x,y)dA_c}, \tag{1}$$

where A_c is the projected frontal area of the obstacle. In other words, aerodynamic porosity determines the portion of the flow that passes through the porous material with respect to the flow that diverges from the obstacle. To estimate α_p, we performed velocity measurements upstream and downstream a single tree that was placed on a raised block in the wind tunnel so that the incident flow was not affected by the boundary layer and the integral at the denominator in Eq. 1 could be replaced by the simple product $U_{ref} \cdot A_c$. Behind the tree (in the first plane not occupied by the tree branches) point velocities were measured on a regular and dense grid and a two-dimensional velocity field was obtained through spatial interpolation. The average velocity was then estimated by integrating the velocity field over the tree silhouette (Fig. 3.b). The mean speed upstream (U_{ref}) and downstream (U_b) the tree were 4.95 m/s and 1.48 m/s, respectively. By means of Eq. 1, we obtained $\alpha_p = 0.3$, a value in line with that of common natural trees, as hollies and cypresses (see square markers in Fig. 3.d from the study of Manickathan et al. (2018)).

The optical porosity β_p is another commonly used parameter to characterize the vegetation and it can be easily estimated by elaborating digital photos (Velarde et al., 2018). It is defined as the ratio between the open surface of a porous material and its total surface. Through a digital elaboration of the photo capturing the frontal view of the model tree (Fig. 3.a), we delimited the silhouette of the tree and obtained its cross-section, $A_c \approx 3.5 \times 10^{-3}$ m^2. Then, we estimated the optical porosity, $\beta_p \approx 0.05$, as the ratio of the number of white pixels to the total number of pixels within the silhouette of the tree. According to the empirical relationship found experimentally by Guan et al. (2003), the optical porosity (β_p) is related to the aerodynamic porosity as:

$$\alpha_p \simeq \beta_p^n, \tag{2}$$

where the exponent n was estimated by Guan et al. (2003) equal to 0.4 for realistic windbreak. Introducing our estimated values for α_p and β_p in Eq. 2, we find $n \approx 0.402$ that is consistent with the cited study. The relation in Eq. 2 can then be conveniently used for deriving the aerodynamic porosity when velocity measurements cannot be directly performed.

The drag coefficient is defined as:

$$c_d = \frac{2F}{\rho_a U_{ref}^2 A_c}, \tag{3}$$

where F is the drag force [N], ρ_a is air density [kg/m^3], U_{ref} is the reference velocity [m/s] for the approaching wind, and A_c is the projected frontal area of the tree [m^2]. The drag force F was measured by means of a load cell, while the velocity U_{ref} was measured with a Pitot tube, as explained in Section 1.2.

In Fig. 3.b, we report the drag coefficient as a function of the wind velocity U_{ref} and Reynolds number Re for four different faces of a single model tree, obtained by rotating the vertical axis of the tree at intervals of 90°. The Reynolds number was calculated as $Re = U_{ref} H_T/\nu$, where H_T is the tree height and ν is the air kinematic viscosity ($\nu \approx 1.55 \times 10^{-5}$ m^2/s at a temperature of 25°C). Except for the values at low speed (where the experimental uncertainty of the

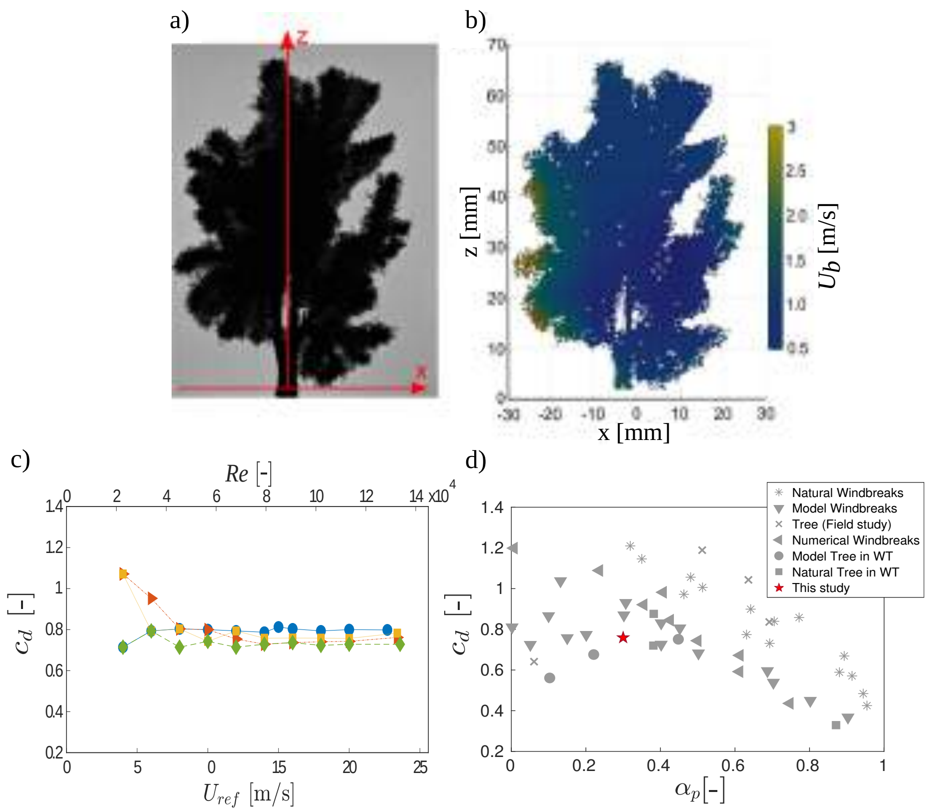

Figure 3: a) Front photo of the model tree. b) 2D velocity field downstream the tree obtained by spatial interpolation of point velocity measurements for the estimation of α_p. c) Drag coefficient as a function of Reynolds number and wind velocity for four different positions (reported by different colours) of a single model tree, obtained by rotating the vertical axis of the tree at 90° intervals. b) Drag coefficient and aerodynamic porosity for various model trees and natural trees. From the study of Manickathan et al. (2018).

measurement is large), the drag coefficient rapidly converges to a constant value around 0.75. As shown in Fig. 3.d, this value is in line with the drag coefficient of natural trees and confirms that the model trees adopted in this study present realistic aerodynamic properties.

We note that natural trees undergo foliage reconfiguration and their drag coefficient decays with increasing wind speed (Manickathan et al., 2018). This is not found in our model trees that do not deform. However, since in this study we focus on moderate velocities in a street canyon, we are not interested in reproducing the flexibility of natural trees.

2.2. Characterization of the boundary layer

To characterize the wind flow over the obstacles, we measured vertical velocity profiles in different positions of the wind tunnel.

The evolution of the boundary layer along the central axis of the wind tunnel (from $x = -1.27$ m to $x = 1.27$ m) is shown in the right part of Fig. 4.a (blue top x-axis). The good overlapping between the curves reveals that the flow is fully developed when it approaches the reference canyon ($x = 0$), i.e. its development in the stream-wise direction is so slow that changes over the fetch can be neglected. As already introduced in Section 1.1, the height of the boundary layer (δ) is around 1.1 m, while the free-stream velocity (U_∞) is around 5 m/s. The characteristic Reynolds numbers based on the obstacle height are $Re_\infty = U_\infty H/\nu \approx 3.3 \times 10^4$ and $Re_H = U_H H/\nu \approx 1.25 \times 10^4$, where U_H is the mean horizontal velocity at $z = H$. These values are sufficiently high to ensure fully-developed turbulent flow. For a square cavity, Allegrini et al. (2013) obtained a Reynolds independent flow for Re_∞ above 1.3×10^4, while Castro and Robins (1977) and Marucci and Carpentieri (2019) showed that the condition was met for Re_H larger than 4000.

Four velocity vertical profiles were measured at different positions within a periodic unit of the urban canopy (see the inset and the velocity profiles on the left side of Fig. 4.a, red bottom x-axis). The influence of the single obstacles is evident in the lower part of the velocity profiles (i.e. the roughness sublayer) where a high scatter can be observed up to $z = 0.15\,\delta$. Above this height, the inertial sublayer develops and the flow variables depend on the vertical coordinate only. In this zone, the mean velocity profile is usually modelled by the logarithmic law:

$$\frac{U}{u^*} = \frac{1}{\kappa} \ln \frac{z - d}{z_0}, \tag{4}$$

where z_0 is the aerodynamic roughness, d is the zero-plane displacement, and u_* is the friction velocity. In the literature, several techniques have been developed to determine the values of these parameters (Raupach et al., 2006). Here, we compare the results from two different methods.

In the first method (Salizzoni et al., 2008), the values of the three parameters were selected so as to minimize the sum of the square difference between the logarithmic velocity profile and the measurements (Fig. 4.b). The logarithmic profile only applies to a fraction of the full velocity profile. Moreover, in urban boundary layers, the inertial sublayer is squeezed by the roughness sublayer that, as seen above, extends beyond the height of the obstacles. This fact makes the delimitation of the inertial zone even more complex than in boundary layers developing over smooth or slightly rough walls. For these reasons, we explored different extensions of the fitted region in the range $0.15 < z/\delta < 0.4$. The resulting parameters were estimated equal to $u_*/U_\infty = 0.051$, $z_0/\delta = 9 \times 10^{-4}$, and $d/\delta = 0.085$.

In the second method, the friction velocity u_* was inferred from the vertical profile of the Reynolds shear stress $-\overline{u'w'}$, where u' and w' are the turbulent fluctuations of the horizontal and vertical velocity, respectively. Except for a thin layer close to the wall, where viscous effects are dominant, the total stress ($\tau = \rho_a u_*^2$) in the surface layer almost matches with the Reynolds stress, which is observed to be almost constant in this layer. Thus, we can write: $\tau = \rho_a u_*^2 = -\rho_a \overline{u'w'}$. Following this method, we have analysed the vertical profile of the Reynolds stresses (Fig. 4.c) which was obtained as a spatial average over the four horizontal positions reported in the inset of Fig. 4.a. A constant-stress region (red filled markers) was detected for $0.14 < z/\delta < 0.36$ and the corresponding u_*/U_∞ was evaluated equal to 0.046. We note that varying the extension of the considered constant-stress region in the range $H/\delta < z/\delta < 0.4$, slight changes (of the order of 4 %) in the estimated value of u_*/U_∞ are found. The aerodynamic roughness ($z_0/\delta = 5 \times 10^{-4}$) and the zero-plane displacement ($d/\delta = 0.1$) were then estimated through a linear regression of the logarithmic law in the semi-log domain.

The results from the two methods are slightly different but in line with previous experimental studies (Rafailidis, 1997; Salizzoni et al., 2008; Garbero et al., 2010). However, since the Reynolds stresses measured by a 45° X-probe HWA are usually underestimated by about 10%-20% (Tutu and Chevray, 1975; Cheng et al., 2007; Marro et al., 2020), we adopt the parameters estimated by minimum mean square error, namely (in non-normalized values) $u^* = 0.29$ m/s, $d = 0.09$ m, $z_0 = 1 \times 10^{-3}$ m.

The vertical profiles of the standard deviation of the velocity components (σ_u, σ_v, and σ_w) and of the turbulent kinetic energy (k) are reported in Figs. 4.d and e. The profiles are representative of a well developed urban boundary layer (Garbero et al., 2010) and can be useful for the implementation and validation of CFD simulations. To this aim, we also provide in Fig. 4.f the vertical profile of the turbulent kinetic energy dissipation rate (ε), which is a fundamental parameter for turbulence closure models. The dissipation rate was estimated from the HWA measurements as:

$$\varepsilon = \frac{15\nu}{U^2}\overline{\left(\frac{\partial u}{\partial t}\right)^2}, \tag{5}$$

by employing the isotropic approximation and Taylor's hypotheses of frozen turbulence (Hinze, 1975). The vertical profile of ε agrees well with the production rate of turbulent kinetic energy, here estimated as $\mathcal{P} \approx -\overline{u'w'}\frac{\partial \overline{u}}{\partial z}$. This shows that in most of the boundary layer, the production and dissipation of turbulent kinetic energy can be assumed to be in local equilibrium (Nironi et al., 2015).

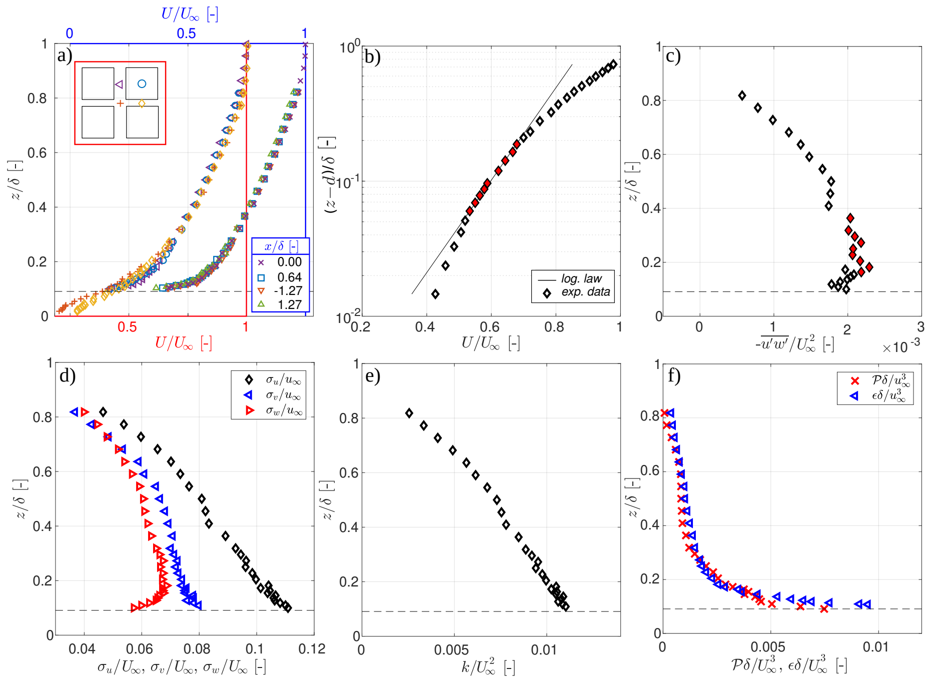

Figure 4: a) Mean velocity at 4 different position in a periodic unit (red bottom x-axis) and at 4 different distances along the streamwise direction of the wind tunnel (blue top x-axis). For the two groups of profiles, a vertical line corresponding the $U/U_\infty = 1$ is reported. The horizontal dashed line corresponds to the canyon roof level (H). b) Mean velocity obtained as average over four different positions. The line represents the logarithmic law with $u_*/U_\infty = 0.051$, $z_0/\delta = 9 \times 10^{-4}$, and $d/\delta = 0.085$. The full symbols indicate the region where the logarithmic law applies. c) Reynolds stresses $-\overline{u'w'}$. The full symbols indicate the constant-stress region. d) Standard deviation of the three velocity components. e) Turbulent kinetic energy. f) Production and dissipation rate of turbulent kinetic energy.

3. Street canyon ventilation

3.1. Mean concentration field

The mean concentration field inside the street canyon was characterized for the three configurations of tree density presented in Fig. 2. As mentioned above (Section 1.2), the concentration of ethane - released from the line source - was measured on around 1000 sampling points (for each configuration) distributed on a three-dimensional grid, by means of a Flame Ionization Detector. The non-dimensional concentration is expressed as $\overline{C^*} = CU_\infty L_s \delta / Q_{et}$, where C is the time-averaged concentration of ethane in each sampling point, L_s is the source length, and Q_{et} is the mass flow rate of ethane. In the following, the results are presented in two-dimensional sections obtained from linear interpolation of the measured data. For a complete visualisation of the concentration field inside the canyon refer to Section 2 of the Supplementary Material.

Figure 5 shows two cross-sections for each configuration of tree density. Panels a-c report the concentration field on a lateral cross-section (y/H ≈-15), whereas panels d-f correspond to the central (around y/H ≈0) cross-section. Regardless of the presence of trees, a clear increase in the concentration from the downwind wall to the upwind wall can be observed in all the sections. This pattern is in accordance with previous studies (Gromke and Ruck, 2007, 2009) and evidences the action of the main recirculating cell of the velocity field inside the canyon: fresh air enters the canyon at the downwind wall and transports the pollutant (emitted in the centre of the street) to the upwind wall, where part accumulates at the lower corner, part is moved outside and part is entrained towards the downwind wall. The horizontal inhomogeneity of the concentration field results in a significant difference in air quality at the pedestrian level (i.e. at $z/H = 0.2$). This difference is accentuated in the presence of trees: in a canyon without vegetation (Fig. 5.a and d), the concentration at the downwind wall is roughly 3 times lower than the one at the upwind wall, while in presence of trees this difference increases up to 8 times in the lateral section (Fig. 5.b and c). We also remark that, for the non-vegetated canyon, the concentration field remains almost unchanged along the longitudinal axis of the canyon (panel a and d) while the presence of trees alters this behaviour: in both the *Half* and *Full* configurations, pollutant concentration in the central section (panel e and f) is significantly lower than in the lateral one (sections b and c).

To better visualize the spatial distribution of the concentration field, we show in Fig. 6 the horizontal section along the canyon axis, at z/H=0.5. The concentration gradient along the x-axis, from the downwind to the upwind wall, is clearly visible in all three configurations. As found above, this gradient is enhanced in the vegetated canyons. Analysing the concentration near the walls (see also the entire cross sections at $x/H = 0.1$ and $x/H = 1.9$ in the Supplementary Material), we find that this is due to an average increase in the concentration at the upwind wall in the vegetated canyons, rather than to a decrease of the concentration at the downwind wall, which remains almost constant in the different configurations. This result is in line with the study of Buccolieri et al. (2009) who found that the presence of trees lead to a significant increase in pollutant concentration at the upwind wall and slight to moderate decrease at the downwind wall.

Figure 6 also shows that along the longitudinal axis (y-axis), the concentration is almost homogeneous in the *Zero* configuration (panel a), except for the low values at the edges of the domain due to the limited length of the linear source. On the other hand, the homogeneity along the y-axis is lost when trees are added. In the *Full* configuration (panel c), it is possible to identify a region with lower concentration in the middle of the canyon and two nearly symmetric accumulation regions at its sides. In the *Half* configuration (panel b), the concentration field is even more heterogeneous and three accumulation regions can be identified. The same spatial distribution can be inferred from Fig. 7, where a vertical section in the middle of the canyon (x/H=1) is represented. Again, we observe a homogeneous concentration field in the empty canyon, while pollution peaks are evident in the *Half* and *Full* configurations. Along the vertical axis, the concentration remains fairly constant. This is typical in the centre of the canyon and was already visible when focusing on vertical profiles at x/H=1 in

Fig. 5. Moving towards the upwind wall (Fig. 8 shows the vertical section at x/H=0.15), however, the concentration is greater at street level and a gradient along the vertical axis emerges.

By averaging the concentration over the vertical direction (z), we obtain (see Fig. 9) the concentration profile along the longitudinal axis (y), in the centre of the canyon (x/H=1). The profiles highlight the transition from an homogeneous concentration in the empty canyon to a spatial distribution exhibiting pronounced peaks in the vegetated canyons. Furthermore, the increment in the number of trees produces a decrease in the minimum concentration in the centre of the canyon and a slight intensification of the maximum values. We note that the cross-sections shown above in Fig. 5 where taken at the minimum ($y/H \approx 0$) and maximum (left side, $y/H \approx -15$) concentration values for each configuration.

Finally, from the characterization of the concentration field along the canyon (Figs. 6-8), some observations on the local effect of trees on pollution can be deduced. For both configurations with trees, the inhomogeneity along the longitudinal axis (y) is maintained along the x-axis (Fig. 6), both near the two rows of trees ($x/H \rightarrow$0 and $x/H \rightarrow$2) and in the centre ($x/H \rightarrow$1). Furthermore, the number of concentration peaks (2 and 3 in the *Full* and *Half* configurations, respectively) and their spacing do not correspond to the number and spacing of the trees, represented by dashed lines in Figs. 6 to 8. These two aspects, namely the concentration inhomogeneity along the y-axis in the centre of the street and the independence of the concentration peaks on tree pattern, suggest that the variation of the concentration field along the canyon is not due to local effects of trees acting as obstacles. Rather, the presence of trees seems to modify the dynamics of flow and dispersion within the whole canyon leading to a different spatial organization of the concentration field at the canyon-scale.

3.2. Vertical exchange velocity

While the previous section highlighted the effect of trees on the spatial pattern of the concentration field, in this section we investigate the effect of veg-

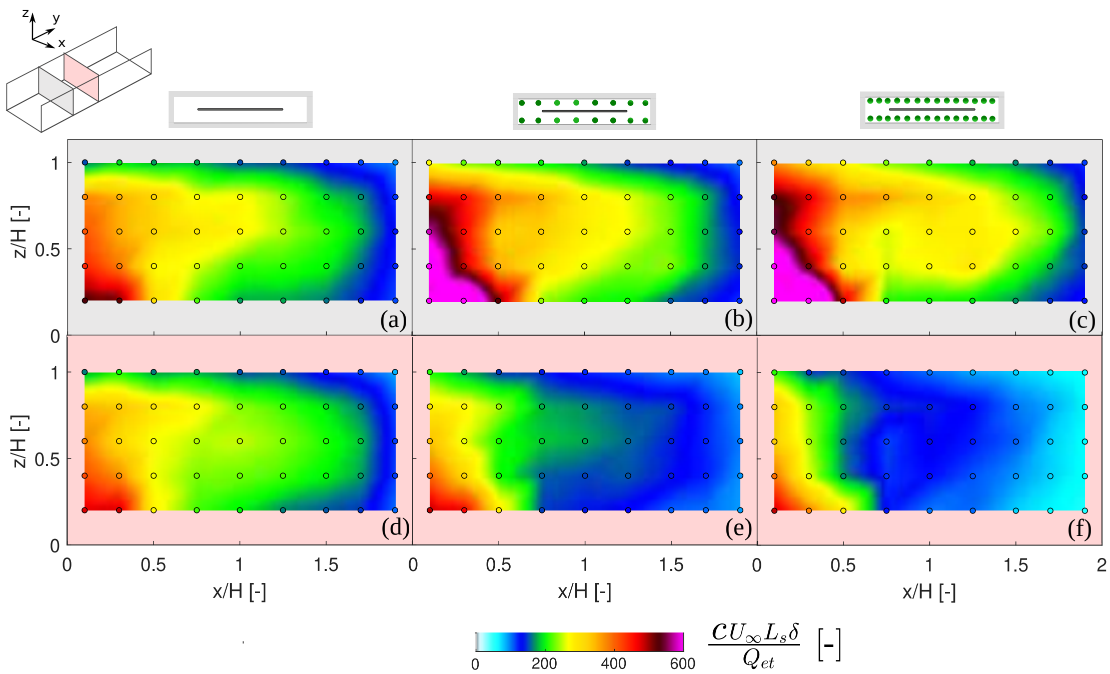

Figure 5: Mean concentration of the passive scalar on a lateral cross-section at $y/H \approx -15$ (first line) and in the centre of the canyon $y/H \approx -0$ (second line). *Zero* (a and d), *Half* (b and e) and *Full* (c and f) configurations are shown. Measurement points are reported as circles colored according to the measured value.

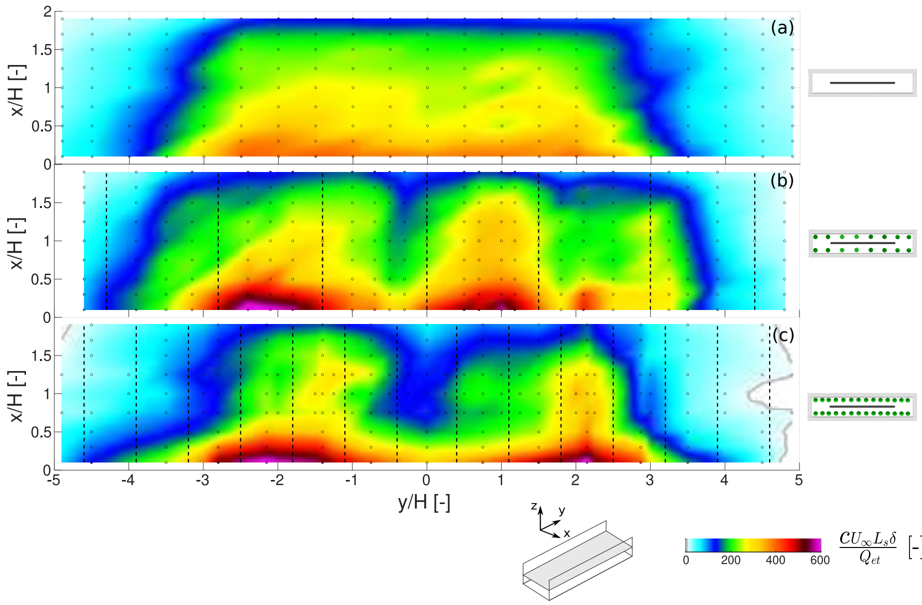

Figure 6: Mean concentration of the passive scalar on the horizontal section at z/H=0.5. *Zero* (a and d), *Half* (b and e) and *Full* (c and f) configurations are shown. The position of trees is represented by dashed lines. Measurement points are reported as circles colored according to the measured value.

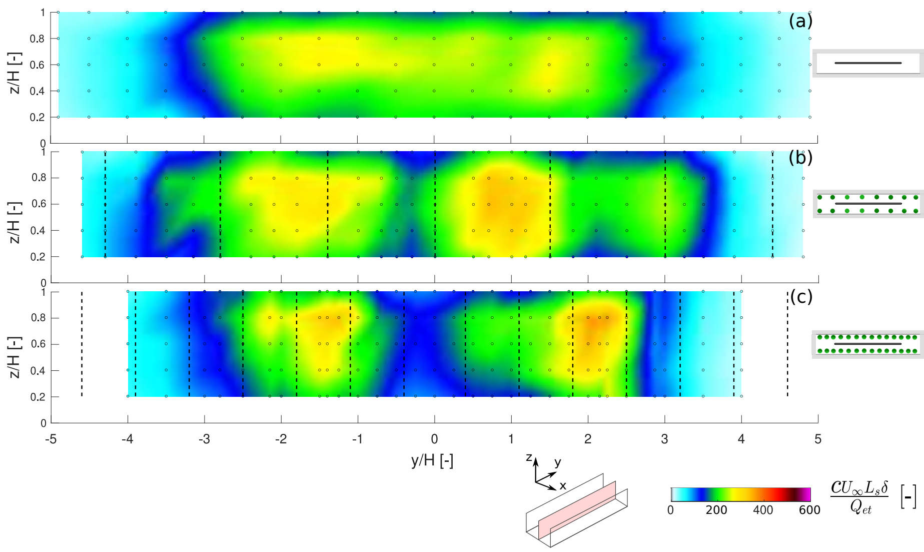

Figure 7: Mean concentration of the passive scalar on a vertical section at x/H=1. *Zero* (a and d), *Half* (b and e) and *Full* (c and f) configurations are shown. The position of trees is represented by dashed lines. Measurement points are reported as circles colored according to the measured value.

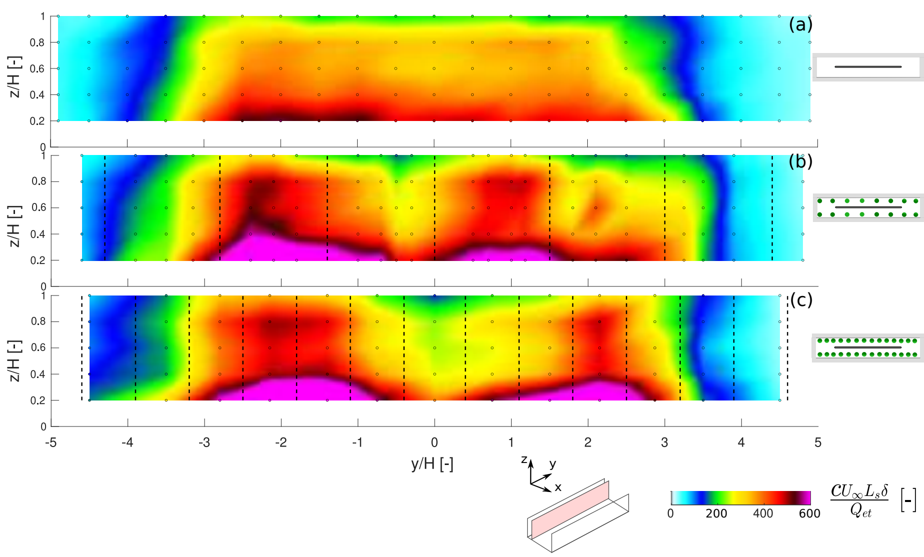

Figure 8: Mean concentration of the passive scalar on a vertical section at x/H=0.15. *Zero* (a and d), *Half* (b and e) and *Full* (c and f) configurations are shown. The position of trees is represented by dashed lines. Measurement points are reported as circles colored according to the measured value.

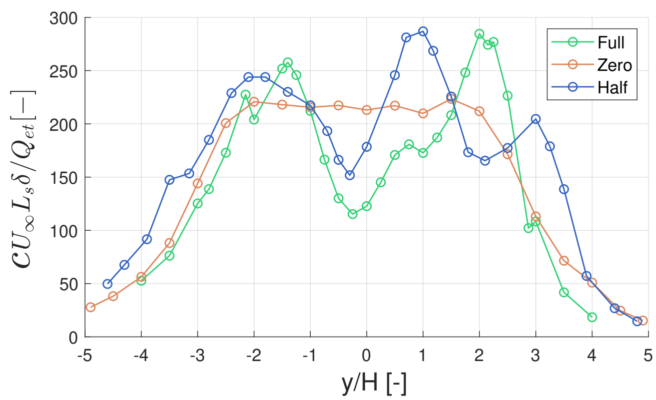

Figure 9: Concentration profile along the canyon axis ($x/H = 1$) for the three configurations of tree density. Each point is obtained as the average concentration along the vertical axis (z).

etation on the ventilation efficiency of the canyon. To this aim, we adopt a box model with one degree of freedom to evaluate the wash-out velocity of the canyon for the different configurations of tree density.

The canyon is described as a unique box with volume-averaged concentration and a domain boundary surface at the roof height (of area $L \cdot W$). The mass balance for the canyon reads:

$$V \frac{\partial C_{vol}}{\partial t} + \int_{-L/2}^{L/2} \int_0^W \left[\overline{wc}\right]_{z=H} dxdy = Q_{et}, \tag{6}$$

where V is the volume of the canyon, Q_{et} is the mass flow rate of ethane at the source, C_{vol} is the mean concentration in the canyon, and $\overline{wc}$ is the mass flux of passive scalar in the vertical direction. This latter is provided by the time-averaged product of the instantaneous vertical velocity w and concentration c. Following Soulhac et al. (2013), the vertical flux at roof level can be parametrized as the product of a bulk exchange velocity u_d and the difference between the concentration within the canyon (C_{vol}) and the concentration in the external flow (C_{ext}):

$$u_d(C_{vol} - C_{ext})WL = \int_{-L/2}^{L/2} \int_0^W \left[\overline{wc}\right]_{z=H} dydx. \tag{7}$$

In steady state conditions (i.e. $\partial C_{vol}/\partial t = 0$) and assuming that C_{ext} is negligible, Eqs. 6 and 7 can be combined, and the exchange velocity expressed as (Salizzoni et al., 2009):

$$u_d = \frac{Q_{et}}{C_{vol} W L}. \tag{8}$$

or in non-dimensional form as:

$$\frac{u_d}{U_\infty} = \frac{L_s \delta}{C^*_{vol} W L}, \tag{9}$$

where C^*_{vol} is the non-dimensional concentration averaged over the volume and L_s is the source length inside the volume. Thanks to this formulation, the vertical exchange velocity can be easily estimated from the quantities measured in the experiment: the flow rate at the source Q_{et} is imposed and monitored by a mass-flow rate controller, while the FID measurements inside the street canyon provide the average concentration in the entire volume (C^*_{vol}).

In this regard, we recall that the choice of reproducing a canyon closed at the lateral edges was made to simplify the estimation of the exchange velocity u_d. Otherwise, in the case of a canyon with lateral street intersections, the mass balance in Eq. 6 would also include the flux of passive scalar along the longitudinal direction (i.e. the mass flux $\overline{vc}$ provided by the transversal velocity v along y and integrated at the lateral boundaries of the domain, at $y = -L/2$ and $y = +L/2$). This additional term would also appear in Eqs. 8 and 9 and thus the estimation of u_d would require additional coupled measures of velocity and concentration. In the case of an infinitely long canyon (i.e. a canyon long as the wind-tunnel width), the balance would be applied to a reference volume since the fine characterization of the entire canyon length would be experimentally unfeasible. Also in this case, the estimate of the transverse mass flux at the lateral boundaries of the reference volume would be necessary to estimate u_d.

The mean concentration within the canyon was estimated with different spatial averaging techniques of the measurements: (i) the rough mean of the data, (ii) the mean weighted by the volume associated to each measurement point, and (iii) the mean over a regular concentration grid obtained from interpolation of the measurements. Table 1 reports the values of C^* obtained with these different methods. The greatest differences in the estimation of C^* are found for the *Full* configuration, where the measurement grid is more irregular due to the presence of trees. In this case, the method adopted for the spatial integration can affect the results. Regardless the method used, we observe that the concentration average in the whole volume of the canyon remains substantially unchanged with the density of trees. This evidences that, while the spatial variation of the concentration field (Figs. 5-8) significantly varies due to the presence of trees, the average pollution level inside the canyon remains almost unaltered. This is a remarkable and unexpected result, as it is generally believed that trees, acting as aerodynamic obstacles, are responsible for the accumulation of pollutants in the street.

To better quantify the effect of trees on street canyon ventilation, we use Eq. 9 to estimate the exchange velocity u_d, starting from C^*_{vol}. The values of u_d are also presented in Table 1 and show, once again, that the influence of trees on ventilation efficiency is almost negligible. Furthermore, a trend of u_d with the vegetation density is absent, being the *Half* configuration the one exhibiting the lowest exchange rate. We also note that the estimated values of u_d are higher with respect to those found by Salizzoni et al. (2009), Soulhac et al. (2013), and Fellini et al. (2020) for a square cavity (H/W=1), confirming that the enlargement of the cavity enhances canyon ventilation.

The values reported in Table 1 have been estimated considering the entire canyon as the reference volume. In Fig. 10, we show how the estimate of u_d varies as a function of the size of the reference volume. To this aim, we consider a reference volume centred at y=0, extended to the entire width (W) and height (H) of the canyon, but of variable length (L_{vol}) along the longitudinal axis (y). For the estimate of u_d by means of Eq. 9, the average concentration is estimated as the mean of the measurement data interpolated over a regular grid ('Interpolation' in Table 1) inside the reference volume, the source length L_s becomes the effective length included inside the reference volume (L'_s in Fig. 10) and the length L is replaced by L_{vol}. For the empty canyon, the exchange rate is almost unchanged as the reference volume increases. This is due to the homogeneity of the concentration field along y. In the *Full* configuration, the

		Rough	Weighted	Interpolation
C^*_{vol} [-]	*Zero*	155.45	162.50	155.43
	Half	198.61	178.75	178.74
	Full	178.76	143.00	162.50
u_d/U_∞ [-]	*Zero*	0.023	0.022	0.023
	Half	0.018	0.020	0.020
	Full	0.020	0.025	0.022

Table 1: Estimate of the volume-averaged (normalised) concentration C^*_{vol} for different spatial averaging techniques of the concentration inside the canyon: (i) rough mean, (ii) mean weighted on the reference volume of each measurement point, and (iii) mean of the three-dimensional interpolated concentration field. The corresponding values of the vertical exchange velocity u_d/U_∞, calculated by means of Eq. 9, are also reported.

velocity u_d is greatly overestimated if a volume less than 40% of the total canyon is considered. The reason for this is that, according to the balance in Eq. 9, the lower concentration in the centre of the canyon results in a misleading high ventilation efficiency. The *Half* configuration shows an intermediate behaviour between the two. This analysis highlights the importance of a characterization of the concentration field on an extended volume for a correct evaluation of the overall ventilation efficiency. To analyse the effect of the presence of trees in the street, characterizing a single two-dimensional section or a limited volume in the middle of the canyon may lead to false conclusions.

4. Discussion about the effect of lateral boundaries

As mentioned above, the canyon geometry with closed extremities was adopted to ensure a correct and straightforward estimate of the ventilation efficiency. However, this geometry is unusual compared to classic experimental investigations (and realistic urban geometries) and could raise the question that the lateral walls modify the flow field and therefore the dispersion process. For this reason, in this section we briefly discuss the effect of the lateral edges of the canyon on the concentration field. To do this, we compare the results pre-

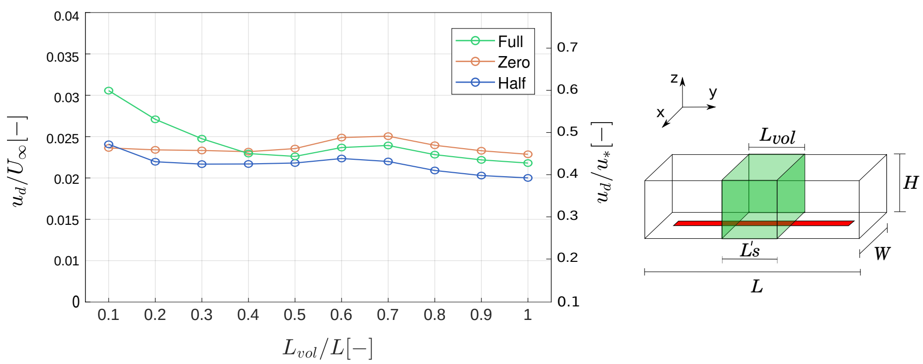

Figure 10: Estimate of the exchange velocity u_d as a function of the length (L_{vol}) of the reference volume along the longitudinal axis of the canyon.

sented in the previous section with concentration measurements performed in the same wind tunnel, with identical experimental conditions, but with slightly different street geometries. We note that these measurements were performed on a coarser grid with respect to that adopted for the investigation of the closed canyon. While these measurements provide a qualitative description, a deep analysis of the influence of lateral boundaries goes beyond the scope of this paper.

In the first laterally-open geometry (Fellini, 2021), the reference canyon is part of the network of streets that reproduces the idealized urban district. The canyon is 50 cm long and is limited laterally by two street intersections (Fig. 11). Although the length-to-width (L/W) ratio is lower and a regular array of building is here present, the street geometry is similar to that adopted by Gromke and Ruck (2007, 2009), where a laterally open canyon is reproduced. Concentration measurements were performed over 4 cross-sections (sections 1 to 4) covering all the canyon length and placed at $y/H \pm 1.88$ and $y/H \pm 0.63$. Results for an empty canyon and a canyon with a full density of trees are presented in panels b and d of Fig. 11, respectively. The density of trees corresponds to the *Full* configuration presented in Section 1.1. Panels c and e refer to the canyon with closed lateral edges and report the concentration measured in the cross-sections taken at the y/H positions closest to those of sections 1 to 4. Without trees, pollution levels are significantly lower in the open canyon (panel b) with respect to the laterally closed one (panel c). This is an expected result, as the formation of corner eddies near the intersections provide additional turbulent exchange that favours the canyon ventilation. Despite this variation in the pollution levels, we observe a similar trend for the concentration that remains almost unchanged along the longitudinal axis. The same observations can be made for the vegetated canyon: the presence of lateral intersections decreases the average concentration in the canyon but the trend along y is similar with open (panel d) and closed ends (panel e). In this case, sections 1 and 4 exhibit an increase in the concentration with respect to section 2 and 3. This trend is in line with the results found in Section 3.1 and suggests that trees induce a three-dimensional concentration field.

A similar comparison is performed for the geometry presented in Fig. 12.a. In this case, the canyon is extended to the entire width of the wind tunnel ($W/H = 35$). The other geometrical properties of the canyon, as well as the experimental conditions, are the same as presented in Section 1.1. Concentration measurements are available in four cross-sections placed in the range at $y/H \pm 1.07$ and $y/H \pm 0.36$. In both the *Zero* and *Full* configurations, the concentration values (panels b and d) are extremely similar to those found in the closed cavity (c and e). The concentration field remains constant along the axis of the canyon in the absence of trees (panel b), while in the *Full* configuration the concentration tends to increase in sections 1 and 4 which are located near the two peaks evident in Fig. 9. We note that the compared sections are not in exactly the same position along the y-axis, the differences being up to 3 cm. This may explain the slightly higher concentration in section 4 of the vegetated canyon (panels d and e). Furthermore, we highlight that in panels c and d the concentration distribution and the effect of the main canyon vortex can be visualized in greater detail due to the higher spatial resolution in the measurements.

The comparisons discussed in this section suggest that the results presented

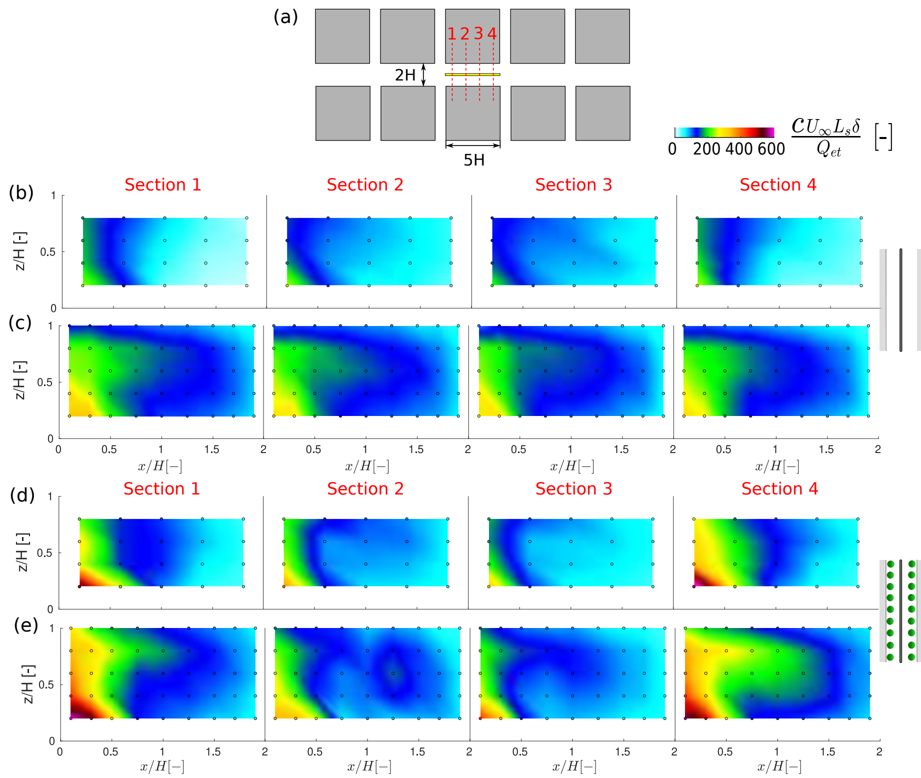

Figure 11: (a) Canyon with street intersections at the lateral extremities. Concentration in 4 cross-sections for the configuration without trees (b) and with dense trees (d). Comparison with the concentration in the closed cavity, in the *Zero* (e) and *Full* configurations.

in Sections 3.1 and 3.2 can be extended, with good approximation, to the standard case of an indefinitely long canyon. The closure of the lateral ends does not seem to alter the ventilation dynamics. The geometry with lateral intersections, on the other hand, presents more marked differences but the presence of trees seems, even in this case, to trigger the same transition from a two-dimensional to a three-dimensional concentration field.

5. Conclusions

We have investigated the effect of trees on ventilation efficiency and pollutant dispersion in an urban street canyon. In a wind tunnel, we have reproduced

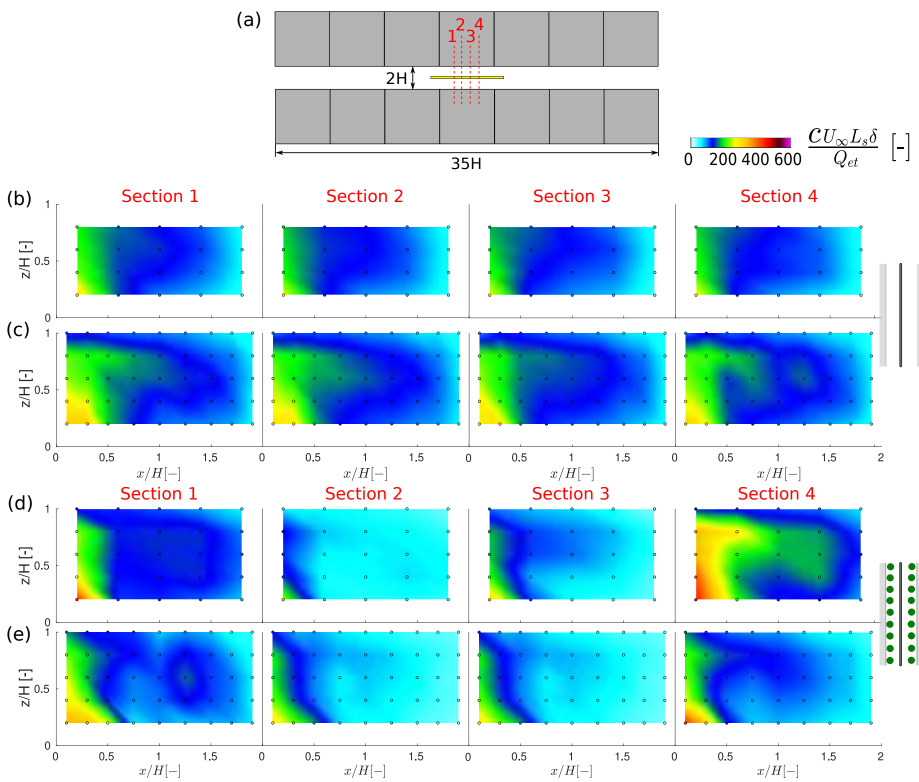

Figure 12: (a) Canyon extended to the width of the wind tunnel. Concentration in 4 cross-sections for the configuration without trees (b) and with dense trees (d). Comparison with the concentration in the closed cavity, in the *Zero* (e) and *Full* configurations.

a well-developed urban boundary layer over an idealized urban district simulated by an array of square blocks. We performed velocity measurements by means of an X-wire HWA in order to provide an accurate description of the flow field above the obstacles. The concentration field was measured by means of a FID within a reference street canyon modelled as a closed cavity oriented perpendicular with respect to the wind direction. Three different configurations of tree density were analysed: a non-vegetated canyon (*Zero* configuration), a canyon with two rows of sparse trees (*Half* configuration), and a canyon with two rows of dense trees (*Full* configuration). The model trees were aerodynamically characterized by means of their drag coefficient and crown porosity.

The results show that the concentration field is homogeneous along the longitudinal axis of the canyon in the *Zero* configuration, and can be considered nearly two-dimensional. On the other hand, the vegetated streets present a remarkable three-dimensional spatial distribution of the concentration field. In particular, concentration peaks alternating with low polluted regions are observed along the canyon both in the *Half* and *Full* configurations and especially at pedestrian level. Moreover, the presence of trees lead to a significant increase of pollutant concentration at the upwind wall of the street, while the average concentration at the downwind wall is almost constant in the different configurations. Despite the great influence of trees on the spatial pattern of pollution, the average concentration in the entire volume of the canyon does not vary with the tree density, highlighting a compensation effect between the different regions of the street.

The ventilation efficiency of the canyon was assessed by estimating the bulk transfer velocity between the canyon and the boundary layer aloft. To this aim, a mass balance within the laterally closed canyon was performed. In line with the result about the mean concentration, the estimated velocity is almost constant among the three configurations, confirming that the vegetation density does not affect the overall ventilation efficiency. On the other hand, we demonstrated that the characterization of the concentration field over an extended reference volume is necessary to accurately estimate the transfer velocity when trees are present.

Finally, we discussed the effect of the canyon lateral extremities on dispersion dynamics. To this aim, we compared the outcomes from two experiments with slightly different canyon geometries. The presence of lateral street intersections increases the ventilation of the canyon and therefore decreases the average pollution levels. However, both in the case of a non-vegetated canyon and in the presence of trees, the trend of the concentration along the longitudinal axis is similar to that found in this study. If we consider a canyon that extends to the entire width of the wind tunnel, the concentration pattern is quite similar to that observed in the configuration with closed ends and longitudinal mass fluxes are quite negligible. Therefore, the results of this study can be generalized to the case of an infinitely long street canyon, which is a classical geometry adopted in both experimental and numerical studies.

To conclude, thanks to the detailed characterization of the concentration field, we showed that trees have a non-trivial effect on the spatial distribution of the pollutant concentration, leading to a highly inhomogeneous scalar field and strong pollution gradients at the pedestrian level. This suggests that the presence of trees affect the turbulent flow field within the canyon. A new measurement campaign is currently underway to investigate the reasons for the formation of pollution peaks in the presence of trees. To this aim, we characterize the structure of the turbulent flow field within the canyon and the vertical turbulent mass fluxes at the roof level. While the vertical exchange velocity u_d is an average quantity over the entire volume, the analysis of the vertical turbulent fluxes should highlight whether there are spatial heterogeneities in the exchange between the canyon and the atmosphere.

Moreover, we found that the presence of two rows of trees does not inhibit the overall canyon ventilation. This result has important implications in practice. The estimated value of the vertical exchange velocity can be included as a constant in parametric models that simulate pollutant dispersion in cities (McHugh et al., 1997; Soulhac et al., 2011; Fellini et al., 2019).

Finally, the huge dataset provided by this experimental study can be of great use for the validation of numerical simulations. To this end, the characterization of the boundary layer and of the aerodynamic properties of trees (described in the Section 2) are fundamental information.

Data availability

The experimental dataset is available on the website: `https://github.com/sfellini/Tree_alpha90_HW05.git`. We provide the concentration data inside the canyon and the characterization of the flow field above the buildings.

Aknowledgements

We would like to express our gratitude to Horacio Correia for the technical support in performing the wind tunnel experiments, and to Alessandro De Giovanni, Giacomo Balestrieri, and Lucas Mechinaud for taking part in the experimental campaign.

References

Abhijith, K., Kumar, P., Gallagher, J., McNabola, A., Baldauf, R., Pilla, F., Broderick, B., Di Sabatino, S., Pulvirenti, B., 2017. Air pollution abatement performances of green infrastructure in open road and built-up street canyon environments–a review. Atmospheric Environment 162, 71–86.

Allegrini, J., Dorer, V., Carmeliet, J., 2013. Wind tunnel measurements of buoyant flows in street canyons. Building and Environment 59, 315–326.

Bozovic, R., Maksimovic, C., Mijic, A., Smith, K., Suter, I., Van Reeuwijk, M., 2017. Blue green solutions. a systems approach to sustainable and cost-effective urban development .

Buccolieri, R., Carlo, O.S., Rivas, E., Santiago, J.L., Salizzoni, P., Siddiqui, M.S., 2022. Obstacles influence on existing urban canyon ventilation and air pollutant concentration: A review of potential measures. Building and Environment , 108905.

Buccolieri, R., Gromke, C., Di Sabatino, S., Ruck, B., 2009. Aerodynamic effects of trees on pollutant concentration in street canyons. Science of the Total Environment 407, 5247–5256.

Buccolieri, R., Salim, S.M., Leo, L.S., Di Sabatino, S., Chan, A., Ielpo, P., de Gennaro, G., Gromke, C., 2011. Analysis of local scale tree–atmosphere interaction on pollutant concentration in idealized street canyons and application to a real urban junction. Atmospheric Environment 45, 1702–1713.

Busca, F., Revelli, R., 2022. Green areas and climate change adaptation in a urban environment: The case study of "le vallere" park (turin, italy). Sustainability 14, 8091.

Carpentieri, M., Hayden, P., Robins, A.G., 2012. Wind tunnel measurements of pollutant turbulent fluxes in urban intersections. Atmospheric Environment 46, 669–674.

Castro, I., Robins, A., 1977. The flow around a surface-mounted cube in uniform and turbulent streams. Journal of fluid Mechanics 79, 307–335.

Chen, J., Black, T., Novak, M., Adams, R., 1995. A wind tunnel study of turbulent airflow in forest clearcuts. Wind and trees , 71–87.

Cheng, H., Hayden, P., Robins, A., Castro, I., 2007. Flow over cube arrays of different packing densities. Journal of Wind Engineering and Industrial Aerodynamics 95, 715–740.

Comte-Bellot, G., 1976. Hot-wire anemometry. Annual review of fluid mechanics 8, 209–231.

Fackrell, J., 1980. A flame ionisation detector for measuring fluctuating concentration. Journal of Physics E: Scientific Instruments 13, 888.

Fellini, S., 2021. Modelling pollutant dispersion at the city and street scales. Ph.D. thesis. Politecnico di Torino & École Centrale de Lyon.

Fellini, S., Ridolfi, L., Salizzoni, P., 2020. Street canyon ventilation: Combined effect of cross-section geometry and wall heating. Quarterly Journal of the Royal Meteorological Society .

Fellini, S., Salizzoni, P., Soulhac, L., Ridolfi, L., 2019. Propagation of toxic substances in the urban atmosphere: A complex network perspective. Atmospheric Environment 198, 291–301.

Garbero, V., Salizzoni, P., Soulhac, L., 2010. Experimental study of pollutant dispersion within a network of streets. Boundary-layer meteorology 136, 457–487.

Georgakis, C., Santamouris, M., 2017. Determination of the surface and canopy urban heat island in athens central zone using advanced monitoring. Climate 5, 97.

Gromke, C., Blocken, B., 2015. Influence of avenue-trees on air quality at the urban neighborhood scale. part i: Quality assurance studies and turbulent schmidt number analysis for rans cfd simulations. Environmental Pollution 196, 214–223.

Gromke, C., Buccolieri, R., Di Sabatino, S., Ruck, B., 2008. Dispersion study in a street canyon with tree planting by means of wind tunnel and numerical investigations–evaluation of cfd data with experimental data. Atmospheric Environment 42, 8640–8650.

Gromke, C., Jamarkattel, N., Ruck, B., 2016. Influence of roadside hedgerows on air quality in urban street canyons. Atmospheric environment 139, 75–86.

Gromke, C., Ruck, B., 2007. Influence of trees on the dispersion of pollutants in an urban street canyon - Experimental investigation of the flow and concentration field. Atmospheric Environment 41, 3287–3302.

Gromke, C., Ruck, B., 2008. Aerodynamic modelling of trees for small-scale wind tunnel studies. Forestry 81, 243–258.

Gromke, C., Ruck, B., 2009. On the impact of trees on dispersion processes of traffic emissions in street canyons. Boundary-Layer Meteorology 131, 19–34.

Gromke, C., Ruck, B., 2012. Pollutant concentrations in street canyons of different aspect ratio with avenues of trees for various wind directions. Boundary-Layer Meteorology 144, 41–64.

Guan, D., Zhang, Y., Zhu, T., 2003. A wind-tunnel study of windbreak drag. Agricultural and forest meteorology 118, 75–84.

Hinze, J., 1975. Turbulence, Second edition. McGraw-Hill, New York.

Huang, Y.d., Li, M.z., Ren, S.q., Wang, M.j., Cui, P.y., 2019. Impacts of tree-planting pattern and trunk height on the airflow and pollutant dispersion inside a street canyon. Building and Environment 165, 106385.

Irwin, H., 1981. The design of spires for wind simulation. Journal of Wind Engineering and Industrial Aerodynamics 7, 361 – 366. doi:https://doi.org/10.1016/0167-6105(81)90058-1.

Janhäll, S., 2015. Review on urban vegetation and particle air pollution–deposition and dispersion. Atmospheric environment 105, 130–137.

Li, H., Zhao, Y., Sützl, B., Kubilay, A., Carmeliet, J., 2022. Impact of green walls on ventilation and heat removal from street canyons: Coupling of thermal and aerodynamic resistance. Building and Environment 214, 108945.

Litschke, T., Kuttler, W., 2008. On the reduction of urban particle concentration by vegetation–a review. Meteorologische Zeitschrift 17, 229–240.

Livesley, S., McPherson, E.G., Calfapietra, C., 2016. The urban forest and ecosystem services: impacts on urban water, heat, and pollution cycles at the tree, street, and city scale. Journal of environmental quality 45, 119–124.

Manickathan, L., Defraeye, T., Allegrini, J., Derome, D., Carmeliet, J., 2018. Comparative study of flow field and drag coefficient of model and small natural trees in a wind tunnel. Urban Forestry & Urban Greening 35, 230–239.

Marro, M., Gamel, H., Méjean, P., Correia, H., Soulhac, L., Salizzoni, P., 2020. High-frequency simultaneous measurements of velocity and concentration within turbulent flows in wind-tunnel experiments. Experiments in Fluids 61, 1–13.

Marucci, D., Carpentieri, M., 2019. Effect of local and upwind stratification on flow and dispersion inside and above a bi-dimensional street canyon. Building and Environment 156, 74–88.

McHugh, C., Carruthers, D., Edmunds, H., 1997. Adms–urban: an air quality management system for traffic, domestic and industrial pollution. International Journal of Environment and Pollution 8, 666–674.

Merlier, L., Jacob, J., Sagaut, P., 2018. Lattice-boltzmann large-eddy simulation of pollutant dispersion in street canyons including tree planting effects. Atmospheric Environment 195, 89–103.

Meroney, R.N., 1968. Characteristics of wind and turbulence in and above model forests. Journal of Applied Meteorology 7, 780–788.

Meroney, R.N., 1980. Wind-tunnel simulation of the flow over hills and complex terrain. Journal of Wind Engineering and Industrial Aerodynamics 5, 297–321.

Meroney, R.N., Pavageau, M., Rafailidis, S., Schatzmann, M., 1996. Study of line source characteristics for 2-d physical modelling of pollutant dispersion in street canyons. Journal of wind Engineering and industrial Aerodynamics 62, 37–56.

Moonen, P., Gromke, C., Dorer, V., 2013. Performance assessment of large eddy simulation (les) for modeling dispersion in an urban street canyon with tree planting. Atmospheric environment 75, 66–76.

Murena, F., Mele, B., 2016. Effect of balconies on air quality in deep street canyons. Atmospheric Pollution Research 7, 1004–1012.

Nironi, C., Salizzoni, P., Marro, M., Mejean, P., Grosjean, N., Soulhac, L., 2015. Dispersion of a passive scalar fluctuating plume in a turbulent boundary layer. part i: Velocity and concentration measurements. Boundary-layer meteorology 156, 415–446.

Oliveira, S., Andrade, H., Vaz, T., 2011. The cooling effect of green spaces as a contribution to the mitigation of urban heat: A case study in lisbon. Building and environment 46, 2186–2194.

Pavageau, M., Schatzmann, M., 1999. Wind tunnel measurements of concentration fluctuations in an urban street canyon. Atmospheric Environment 33, 3961–3971.

Rafailidis, S., 1997. Influence of building areal density and roof shape on the wind characteristics above a town. Boundary-layer meteorology 85, 255–271.

Raupach, M., Hughes, D., Cleugh, H., 2006. Momentum absorption in rough-wall boundary layers with sparse roughness elements in random and clustered distributions. Boundary-Layer Meteorology 120, 201–218.

Salim, S.M., Cheah, S.C., Chan, A., 2011. Numerical simulation of dispersion in urban street canyons with avenue-like tree plantings: comparison between rans and les. Building and Environment 46, 1735–1746.

Salizzoni, P., Soulhac, L., Mejean, P., 2009. Street canyon ventilation and atmospheric turbulence. Atmospheric Environment 43, 5056–5067.

Salizzoni, P., Soulhac, L., Mejean, P., Perkins, R.J., 2008. Influence of a two-scale surface roughness on a neutral turbulent boundary layer. Boundary-layer meteorology 127, 97–110.

Soulhac, L., Perkins, R.J., Salizzoni, P., 2008. Flow in a street canyon for any external wind direction. Boundary-Layer Meteorology 126, 365–388.

Soulhac, L., Salizzoni, P., Cierco, F.X., Perkins, R., 2011. The model SIRANE for atmospheric urban pollutant dispersion; part I, presentation of the model. Atmospheric Environment 45, 7379–7395.

Soulhac, L., Salizzoni, P., Mejean, P., Perkins, R., 2013. Parametric laws to model urban pollutant dispersion with a street network approach. Atmospheric Environment 67, 229–241.

Stacey, G., Belcher, R., Wood, C., Gardiner, B., 1994. Wind flows and forces in a model spruce forest. Boundary-Layer Meteorology 69, 311–334.

Tritton, D.J., 2012. Physical fluid dynamics. Springer Science & Business Media.

Tutu, N.K., Chevray, R., 1975. Cross-wire anemometry in high intensity turbulence. Journal of Fluid Mechanics 71, 785–800.

Velarde, J.G., Blanco, J.H., Aliseda, J.M., 2018. Estimation of optical porosity or canopy structure of two species of tree with hemispherical and vertical images. WSEAS Transactions on Environment and Development 14, 112–124.

Vidali, C., Marro, M., Correia, H., Gostiaux, L., Jallais, S., Houssin, D., Vyazmina, E., Salizzoni, P., 2022. Wind-tunnel experiments on atmospheric heavy gas dispersion: Metrological aspects. Experimental Thermal and Fluid Science 130, 110495.

Vos, P.E., Maiheu, B., Vankerkom, J., Janssen, S., 2013. Improving local air quality in cities: to tree or not to tree? Environmental pollution 183, 113–122.

Vranckx, S., Vos, P., Maiheu, B., Janssen, S., 2015. Impact of trees on pollutant dispersion in street canyons: A numerical study of the annual average effects in antwerp, belgium. Science of the Total Environment 532, 474–483.